The Astrophysical Journal Letters, 723:L154–L158, 2010 November 10 doi:10.1088/2041-8205/723/2/L154

QUIET-SUN INTENSITY CONTRASTS IN THE NEAR-ULTRAVIOLET AS MEASURED FROM SUNRISE

J. Hirzberger[1], A. Feller[1], T. L. Riethmüller[1], M. Schüssler[1], J. M. Borrero[1,2], N. Afram[3], Y. C. Unruh[3], S. V. Berdyugina[2], A. Gandorfer[1], S. K. Solanki[1,4], P. Barthol[1], J. A. Bonet[5], V. Martínez Pillet[5], T. Berkefeld[2], M. Knölker[6], W. Schmidt[2], and A. M. Title[7]

[1] Max-Planck-Institut für Sonnensystemforschung, D-37434 Katlenburg-Lindau, Germany; hirzberger@mps.mpg.de
[2] Kiepenheuer-Institut für Sonnenphysik, D-79104 Freiburg, Germany
[3] Astrophysics Group, Blackett Laboratory, Imperial College, London SW7 2AZ, UK
[4] School of Space Research, Kyung Hee University, Yongin, Gyeonggi 446-71, Republic of Korea
[5] Instituto de Astrofísica de Canarias, E-38200 La Laguna, Spain
[6] High Altitude Observatory, National Center for Atmospheric Research, Boulder, CO 80307, USA
[7] Lockheed Martin Solar and Astrophysics Laboratory, Palo Alto, CA 94305, USA
Received 2010 June 16; accepted 2010 August 19; published 2010 October 15

ABSTRACT

We present high-resolution images of the Sun in the near-ultraviolet spectral range between 214 nm and 397 nm as obtained from the first science flight of the 1 m Sunrise balloon-borne solar telescope. The quiet-Sun rms intensity contrasts found in this wavelength range are among the highest values ever obtained for quiet-Sun solar surface structures—up to 32.8% at a wavelength of 214 nm. We compare the rms contrasts obtained from the observational data with theoretical intensity contrasts obtained from numerical magnetohydrodynamic simulations. For 388 nm and 312 nm the observations agree well with the numerical simulations whereas at shorter wavelengths discrepancies between observed and simulated contrasts remain.

Key words: Sun: atmosphere – Sun: general – Sun: granulation

1. INTRODUCTION

Quiet-Sun intensity fluctuations provide fundamental information on the thermal structure of the convective overshoot region at the solar surface. A large number of measurements of the quiet-Sun intensity fluctuations have been made in the visible spectral range, starting in the 1950s (Frenkiel & Schwarzschild 1955) and reaching to comparisons between recent seeing-free observations from the Solar Optical Telescope (SOT) on the *Hinode* satellite, which provide contrast values comparable to those from state-of-the-art numerical simulations (e.g., Danilović et al. 2008; Mathew et al. 2009; Wedemeyer-Böhm & Rouppe van der Voort 2009). Overviews of the results of former measurements are given by Beckers & Parnell (1969) and Sánchez Cuberes et al. (2000). Although many intensity contrast measurements are based on data obtained after careful correction of atmospheric and/or instrumental effects, it turns out that insufficient knowledge of optical aberrations and stray light are still the major obstacles for accurate contrast measurements.

In the near-ultraviolet (NUV), the intensity fluctuations of the solar surface region have been hitherto largely unknown, owing to the lack of reliable imaging data. The strong dependence of the Planck function in the NUV to the temperature makes the intensity highly sensitive to temperature fluctuations. Therefore, intensity contrasts also represent important diagnostics to probe the validity of numerical simulations of convection at granular scales.

From an observational point of view, it is well known that seeing effects and stray light contributions increase toward shorter wavelengths. Ground-based NUV observations are, additionally, hampered by strong atmospheric absorption (mainly by stratospheric ozone). Below the atmospheric cutoff at about 315 nm (see Gandorfer 2005), observations cannot be carried out from the ground.

In the present study, we show for the first time high-resolution imaging data and intensity fluctuations in the NUV region down to 214 nm. These data were obtained during the first science flight of the balloon-borne 1 m Sunrise observatory (see Barthol et al. 2010; Martínez Pillet et al. 2010; Berkefeld et al. 2010; Solanki et al. 2010). We present disk-center quiet-Sun NUV intensity contrasts obtained with the Sunrise Filter Imager (SuFI; see Gandorfer et al. 2010) on board Sunrise.

2. OBSERVATIONS

The first science flight of the balloon-borne Sunrise telescope was carried out between 2009 June 8 and June 13, from Kiruna, Sweden to Somerset Island, Canada. The average cruise altitude was about 36 km, i.e., at the upper boundary of the stratospheric ozone layer, so that high-resolution images in the NUV could be obtained. The spectral regions observed by SuFI are 214 nm, 300 nm, 312 nm (close to the band head of the OH molecule), 388 nm (band head of the CN molecule), and 396.8 nm (Ca II *H* line core). The widths (FWHM) of the corresponding SuFI filters are 10 nm, 5 nm, 1.2 nm, 0.8 nm, and 0.18 nm, respectively. The passbands within CN and OH band heads were selected because of their high temperature sensitivity, especially UV OH lines which are favorable for imaging of both the quiet photosphere and sunspots (Berdyugina et al. 2003). The filters are mounted in a filter wheel that allows for sequential observations of the five wavelength channels.

SuFI is equipped with a 2k × 2k CCD detector (PixelVision BioXight) at an effective focal length of 121 m. The camera pixel pitch is 12 μm corresponding to 0.″0207 (at 300 nm) on the sky. For post-facto correction of low-order optical aberrations by means of phase-diversity (PD) wave front sensing, SuFI was equipped with a device providing a focused and a defocused image, each on one half of the detector. The effective field of view (FOV) is thus limited to about 15″ × 40″.

The exposure times for the SuFI observations were strongly wavelength dependent and ranged from 75 ms in the CN channel up to 30 s in the 214 nm channel. In this latter channel, the intensity level was high enough for detection only

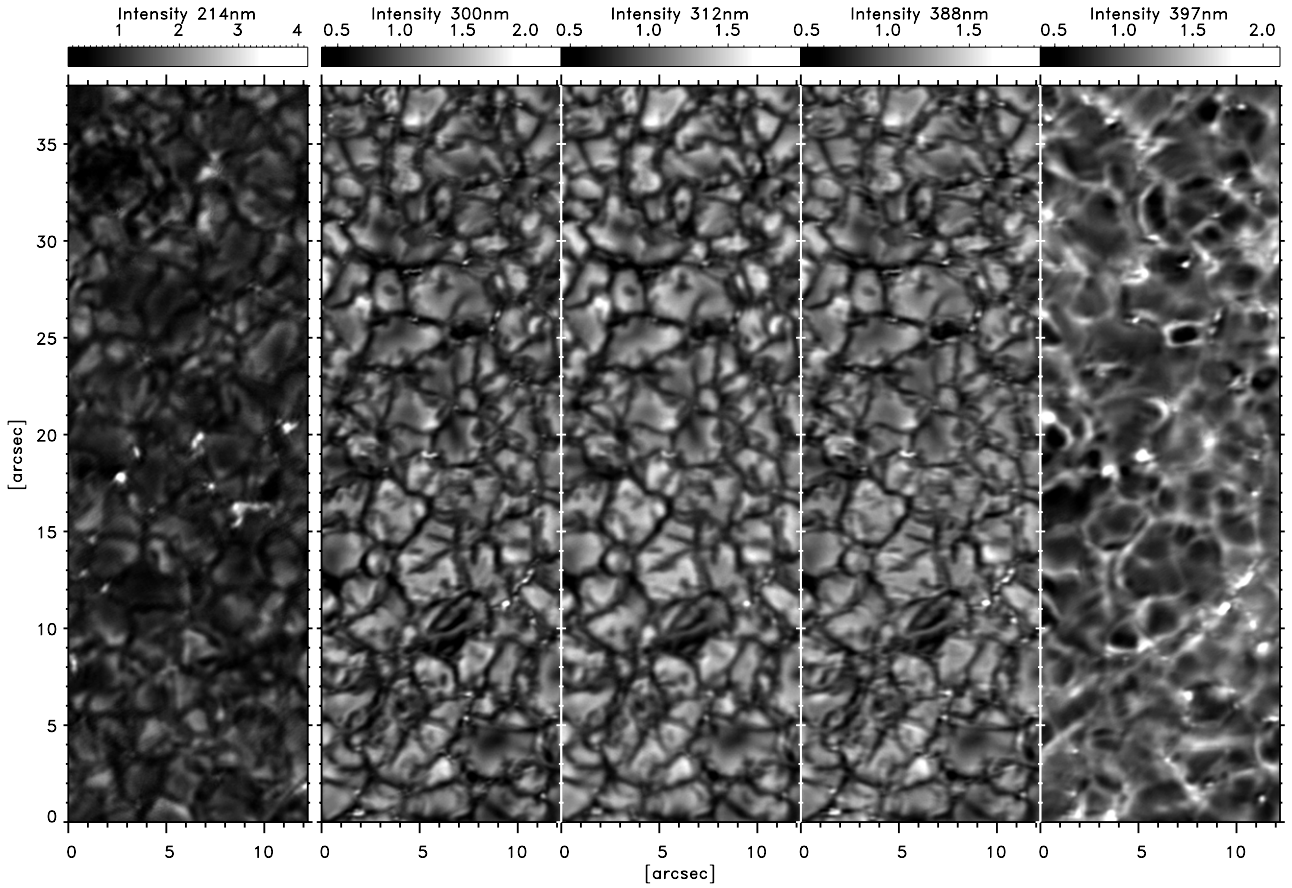

Figure 1. Examples of PD-reconstructed (level 2) images obtained in the five SUNRISE/SuFI wavelength channels. The displayed image in the leftmost panel (214 nm) was obtained on 2009 June 9, 14:59:24 UT, and the other images on June 11, 20:07:41 UT (300 nm), 20:07:42 UT (312 nm), 20:07:38 UT (388 nm), and 20:07:39 UT (397 nm). All images show fields of quiet granulation near the disk center. The intensities have been normalized to the mean intensity $\bar{I}$ over the FOV and the scales have been limited to $\bar{I} \pm 10\sigma$ (214 nm) and $\bar{I} \pm 5\sigma$ (all other channels), respectively, where σ denotes the standard deviation of the corresponding intensity.

around maximum solar elevation and maximum balloon altitude. Therefore, observations in the 214 nm channel were only carried out around local noon.

Here, we show data obtained on 2009 June 11, between 20:00 UT and 21:00 UT (300 nm, 312 nm, 388 nm, and 397 nm) and on 2009 June 9, between 14:00 UT and 15:00 UT (all SuFI channels). Examples of single images obtained in the five SuFI wavelength channels are shown in Figure 1.

3. DATA ANALYSIS

The raw ("level 0") SuFI images were corrected for dark and flat fields. Dedicated flat-field images were obtained by moving the telescope during exposure. For flat-field correction of the science images, accumulations of all flat-field and science images obtained in an interval of ±2 hr around the observation time were used. In addition, clusters of bad detector pixels were eliminated by applying a local median filter. Residual inhomogeneities originating from scratches at the entrance window of the SuFI camera were removed by local smoothing using low-pass filters.

The flat- and dark-field-corrected SuFI images (henceforth labeled as "level 1" data) were reconstructed by means of a PD algorithm. We used a PD code originally described by Löfdahl & Scharmer (1994) and further developed as described by Bonet et al. (2004) and Vargas Domínguez (2008). In order to optimize the reconstruction of the SuFI data, several additional features were included, which will be described together with a performance study of the new PD code in a forthcoming publication (Hirzberger et al. 2010).

In contrast to ground-based observations, the contribution of atmospheric influences to the total wave front aberrations at balloon altitudes is small compared with instrumental effects. Therefore, we expect isoplanatic conditions, i.e., constant wave front aberration across the SuFI FOV. Temporal variations of the wave front deformations are assumed to arise only from changes of the instrument's temperatures and from slowly varying mechanical deformations, which both are mainly correlated with the solar elevation. These assumptions allow a homogeneous reconstruction of the SuFI images. We thus included a procedure, which permits averaging the fitted Zernike coefficients across the entire FOV as well as over all images within a certain time span (usually 1 hr). Subsequently, all images taken during this time span were reconstructed with constant and highly reliable wave front errors. PD reconstruction of individual images is, henceforth, denoted as "level 2" reduction, while images reconstructed with averaged wave front errors are labeled as "level 3."

4. RESULTS

4.1. Disk-center Intensity Contrasts

The quiet-Sun disk-center rms intensity contrasts, $\delta I_{\rm rms}$, derived from the data obtained on 2009 June 11 are plotted in Figure 2. In each spectral channel, for 180 consecutive images (approximately 24 minutes) the image stabilization

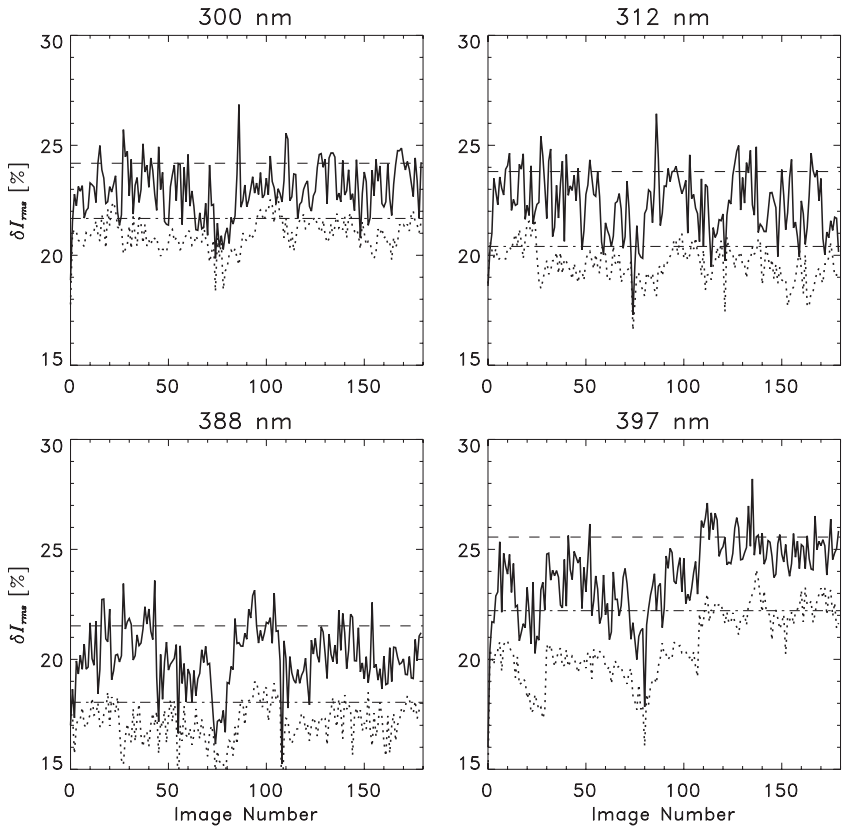

Figure 2. rms intensity contrasts of 180 images in each of four wavelength channels, obtained on 2009 June 11, between 20:00 and 21:00 UT. Solid lines correspond to level-2 data and dotted lines refer to level-3 data. The dashed and dash-dotted horizontal lines lie one standard deviation above the mean contrast of the level-2 and level-3 images, respectively. In the 397 nm band, the contrast is slightly higher in the second half of the image series than in the first half since the FOV had moved by a few arcseconds on the solar disk.

system (SUNRISE Correlating Wavefront Sensor; see Berkefeld et al. 2010) was locking in closed loop. The obtained intensity contrasts show considerable temporal fluctuations which are partially caused by the evolution of the solar structures and *p*-modes but also by a variation of the image quality. The image quality is affected, first, by the limited overall stability given by the gondola pointing and the image stabilization in the presence of wind gusts and vibrations (Berkefeld et al. 2010), and, secondly, by residual artifacts, such as scratches and bad pixels in the level-1 images (see Section 3), which are amplified by the PD reconstruction. After visual inspection, the influence of the latter is considered to be negligible in the data presented here.

In addition to the temporal fluctuations, a rather constant offset of approximately 2%–3% (depending on wavelength) of the intensity contrasts from level-2 to level-3 data is evident. This offset is expected since for the level-2 data always the local best fits to the wave front aberrations are used for reconstruction (which also may cause local over-reconstructions), whereas the averaged wave fronts used for reconstructing the level-3 data may locally underestimate the wave front errors (e.g., due to a small amount of anisoplanatism).

Irrespective of the effect of the image processing methods, the photospheric intensity contrasts shown in Figure 2 are among the highest quiet-Sun contrasts ever measured. The contrast variations within the time series are to a lesser extent related to granular evolution than to the varying image quality due to residual pointing errors. This sometimes leads to artifacts due to local over-reconstruction and thus to unrealistically high contrast values. In the majority of images, this effect, however, tends to result in reduced intensity contrasts (by smearing out solar surface structures). In order to allow for this systematic reduction of contrasts and to clip outliers, we consider the "mean-plus-one-sigma" values, $\langle \delta I_{\rm rms} \rangle + \sigma$, as reliable maximum contrast measurements. Here, $\langle \delta I_{\rm rms} \rangle$ denotes the temporally averaged rms contrast and σ denotes the corresponding standard deviation. The mean-plus-one-sigma values are overplotted in Figure 2 and given in Table 1.

Figure 3 shows the intensity contrasts of 15 images from the 214 nm and 300 nm channels of the June 9 data. As a result of the long exposure time at 214 nm, the number of reliable images obtained during the observing period is limited to that small number. The mean-plus-one-sigma rms contrasts of the June 11 data are marked by arrows. Due to higher residual pointing errors, which caused some smearing of the images, the June 9 data are of slightly worse quality than the June 11 data. This particularly affects the 214 nm data. Nevertheless, the obtained intensity contrasts in the 214 nm channel are the highest photospheric quiet-Sun contrasts ever measured.

4.2. Intensity Contrasts from Simulations

In order to compare with the measured intensity contrasts, we have calculated NUV intensity maps from numerical magnetohydrodynamic (MHD) simulations of the quiet solar photosphere (Vögler et al. 2005). We used snapshots from a simulation run with a mean vertical magnetic field strength of $\langle B_z \rangle = 50$ G and a horizontal cell size of 20.8 km. The intensity maps were calculated by using the spectral synthesis code ATLAS9 (Kurucz 1993), which specifies the opacity distribution functions (ODFs; Strom & Kurucz 1966) in the SuFI 300 nm, 312 nm, and 388 nm channels. With the current implementation

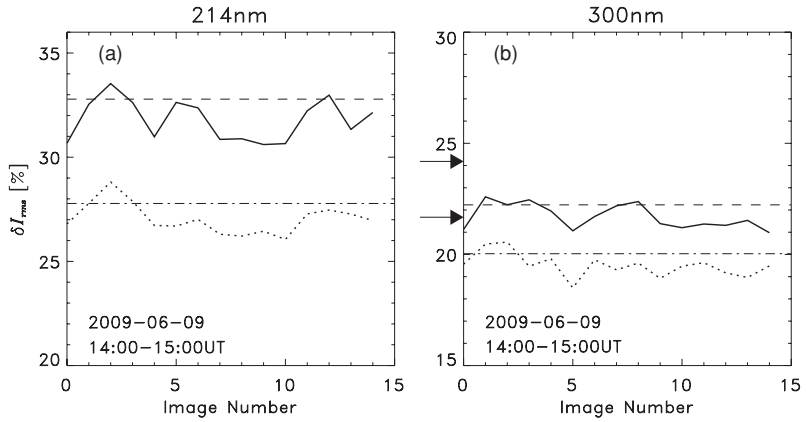

Figure 3. rms intensity contrasts of 15 images taken in the 214 nm (panel (a)) and 300 nm (panel (b)) wavelength channels, obtained on 2009 June 9, between 14:00 and 15:00 UT. Solid lines correspond to level-2 data and dotted lines refer to level-3 data. The dashed and dash-dotted horizontal lines show the mean-plus-one-sigma values of level-2 and level-3 images, respectively. For comparison, the mean-plus-one-sigma values obtained from the June 11 300 nm data are indicated by arrows.

Table 1
Mean-plus-one-sigma Values of $\delta I_{\rm rms}$ (see Figures 2 and 3) and Mean $\delta I_{\rm rms}$ Resulting from MHD Simulation Data (in %)

λ	June 9		June 11		MHD		MHD Stray Light	
(nm)	Level 2	Level 3	Level 2	Level 3	ODF	SPINOR	ODF	SPINOR
214	32.79 (31.80 + 0.98)	27.78 (27.05 + 0.73)	...	...	61.27[a]	...	...	...
300	22.23 (21.63 + 0.60)	20.03 (19.52 + 0.52)	24.19 (22.98 + 1.21)	21.67 (20.94 + 0.73)	30.76	...	25.50	
312	21.91 (20.84 + 1.07)	19.45 (18.79 + 0.66)	23.81 (22.34 + 1.47)	20.40 (19.58 + 0.82)	28.34	...	22.03	...
388	19.16 (18.28 + 0.89)	17.27 (16.73 + 0.55)	21.52 (20.09 + 1.43)	18.05 (17.11 + 0.94)	23.94	25.27	18.60	19.93
397	22.64 (21.33 + 1.30)	20.11 (19.19 + 0.92)	25.56 (23.81 + 1.75)	22.22 (20.60 + 1.61)	...	...	...	...

Notes. In the rightmost two columns, mean $\delta I_{\rm rms}$ of MHD data convolved with preliminary estimated levels of scattered light are given.
[a] Mean $\delta I_{\rm rms}$ at 220 nm.

for computing ODFs, we are unable to calculate reliable intensities below a wavelength of 220 nm. In order to estimate the simulated contrast at 214 nm, we tentatively applied the ODF for 220 nm to the MHD snapshots. In addition, in the SuFI 388 nm channel, a full spectral synthesis with the SPINOR code (Solanki 1987; Frutiger et al. 2000; Berdyugina et al. 2003), including all available atomic and molecular line parameters within the SuFI 388 nm spectral bandpass, has been performed.

Nine synthetic intensity images at 300 nm and the corresponding $\delta I_{\rm rms}$ for all SuFI channels are shown in Figure 4. Owing to the small area (6 Mm × 6 Mm) of the MHD box, the simulated contrasts show a temporal variation with a standard deviation of about 1% (except for the 220 nm spectral region where the value is about 3%). The contrasts obtained with SPINOR in the 388 nm channel are consistently about 1.3% higher than those obtained by using ODFs. This small difference, comparable to the temporal variation of $\delta I_{\rm rms}$, indicates that the ODF-based spectral synthesis in the other spectral channels may not be completely unrealistic, although NLTE effects have not been taken into account. The mean contrasts obtained from the MHD simulations are also given in Table 1.

5. DISCUSSION AND CONCLUSIONS

The NUV intensity contrasts obtained from SUNRISE/SuFI data are systematically lower than the values from MHD simulations by several percent (but nearly a factor of two at 214 nm). Since the spatial resolution of both data sets is similar and because the instrumental aberrations have been removed by means of PD reconstruction, three possible sources for the discrepancy remain: (1) inaccurate physics in the simulations, (2) omission of NLTE effects in the intensity calculations, and (3) scattered light. Before we can estimate the importance of NLTE effects or the need to improve the simulations, we need to judge the influence of scattered light on the measured contrasts.

The amount of scattered light in the SuFI data has not yet been fully assessed. First estimates for the 300 nm, 312 nm, and 388 nm SuFI channels were derived from limb observations. The stray light components of the modulation transfer function obtained from limb profiles at the different wavelengths were applied to the numerical simulations to estimate the effect of stray light on the rms intensity contrasts (see Table 1; details will be presented by A. Feller et al. 2010, in preparation). For 214 nm and 397 nm we were not able, yet, to obtain a stray light estimate due to the lack of limb observations (214 nm) and due to the ubiquitous presence of spicules (397 nm). At 312 nm and 388 nm, the synthetic images after stray light contamination display contrast values that lie between the level-2 and the level-3 data. At these wavelengths, the simulations thus give results consistent with the measurements. At 300 nm, the simulations give a value of 25.5% that is still 1.3% higher than the 24.2% obtained from the level-2 data.

Estimates of scattered light contributions in (also seeing free) data obtained with *Hinode*/SOT were carried out by Mathew et al. (2009) and Wedemeyer-Böhm & Rouppe van der Voort (2009). They found a significant increase of the intensity contrasts in the visible *Hinode* channels, after deconvolving with point-spread functions for scattered light. For the 388 nm spectral region, Mathew et al. (2009) found a quiet-Sun intensity contrast of 21.8% after removing scattered light, which is very similar to the mean-plus-one-sigma value of our level-2 data from 2009 June 11 (cf. Table 1). Therefore, we conclude that after applying stray light correction to the SuFI 388 nm data, the obtained contrasts will exceed those obtained by Mathew et al.

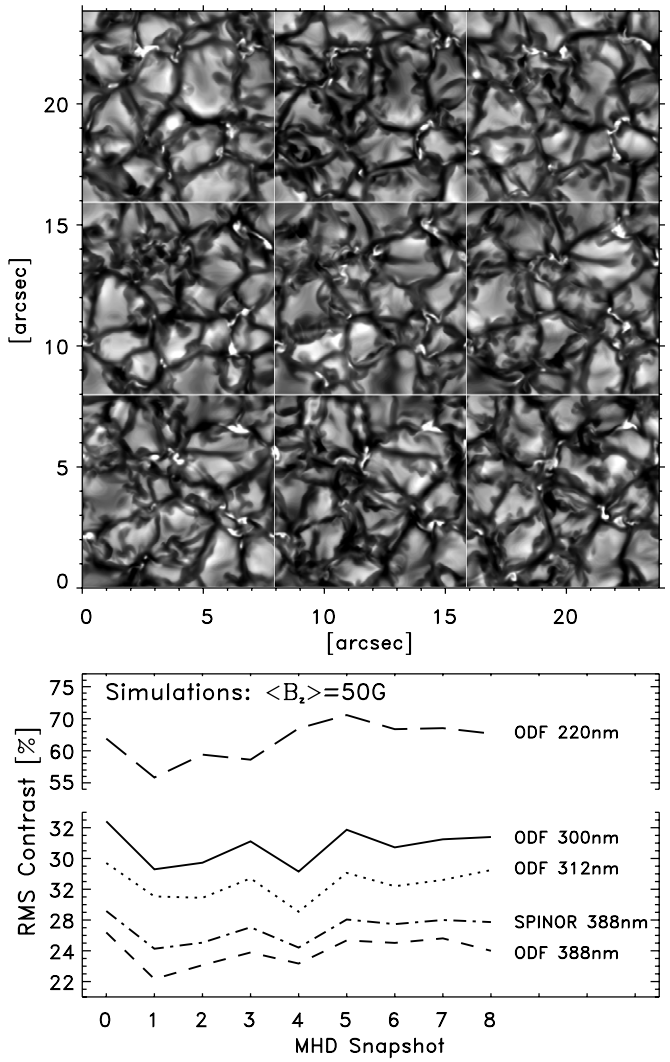

Figure 4. Upper panel: nine brightness images at 300 nm from an MHD simulation with a mean vertical field strength of $\langle B_z \rangle = 50$ G; lower panel: corresponding $\delta I_{\rm rms}$ calculated for four of the five SuFI spectral channels, using two different methods for 388 nm (ODF-based and full spectral synthesis). Since ODFs do not allow reliable intensity calculations at 214 nm, the computations have been carried out at the nearest wavelength at which they are better established, 220 nm.

(2009) from *Hinode* data and will be comparable to synthetic contrasts achieved from MHD data.

The consistency between the measured and the numerically simulated contrasts indicates that the temperature fluctuations in the lower photosphere are correctly described by the hydrodynamical simulations, which predict values of $\delta T_{\rm rms}$ between 2% and 5% on surfaces of constant optical depth (at 500 nm) between $\tau_{500} = 1$ and $\tau_{500} = 0.01$. Taken together with the reproduction of shifts and asymmetries of spectral lines (e.g., Nordlund et al. 2009) and inverse granulation (Cheung et al. 2007) by simulation results, our contrast data thus provide evidence for an extension of the convective overshoot to a height of roughly 300 km above the average level of optical depth unity, at which height the rms fluctuations of the vertical velocity reach a local minimum after a steep decrease (by about a factor of four) from their maximum slightly below the visible surface (optical depth unity).

Direct translation of rms contrasts into, e.g., temperature stratification of the solar photosphere can be carried out only by means of simplified models estimating the brightness temperature of atmospheric features (e.g., Solanki & Unruh 1998; Sobotka et al. 2000). In the NUV, the rms intensity contrast of broadband images as obtained with SUNRISE/SuFI is, however, only partly a function of height. It depends just as much on the temperature sensitivity of the Planck function and of the lines in the SuFI passbands, the atomic species, ionization stages, and in the case of molecular transitions, the dissociation energy of the molecules.

In summary, we conclude that the data obtained from the first science flight of SUNRISE/SuFI are of resounding quality. They show the highest quiet-Sun photospheric intensity contrasts ever measured, even without correcting for scattered light.

The German contribution to SUNRISE is funded by the Bundesministerium für Wirtschaft und Technologie through Deutsches Zentrum für Luft- und Raumfahrt e.V. (DLR), grant number 50 OU 0401, and by the Innovationsfond of the President of the Max Planck Society (MPG). The Spanish contribution has been funded by the Spanish MICINN under projects ESP2006-13030-C06 and AYA2009-14105-C06 (including European FEDER funds). The HAO contribution was partly funded through NASA grant NNX08AH38G. This work has been partially supported by the WCU grant (No. R31-10016) funded by the Korean Ministry of Education, Science and Technology. N.A. and Y.C.U. acknowledge the NERC SolCli consortium grant. S.V.B. acknowledges the EURYI (European Young Investigator) Award provided by the ESF (see www.esf.org/euryi) and the SNF grant PE002-104552. The National Center for Atmospheric Research is sponsored by the National Science Foundation.

REFERENCES

Barthol, P., et al. 2010, Sol. Phys., in press (arXiv:1009.2689)
Beckers, J. M., & Parnell, R. L. 1969, Sol. Phys., 9, 39
Berdyugina, S. V., Solanki, S. K., & Frutiger, C. 2003, A&A, 412, 513
Berkefeld, T., et al. 2010, Sol. Phys., in press (arXiv:1009.3196)
Bonet, J. A., Márquez, I., Muller, R., Sobotka, M., & Tritschler, A. 2004, A&A, 423, 737
Cheung, M. C. M., Schüssler, M., & Moreno Insertis, F. 2007, A&A, 461, 1163
Danilović, S., Gandorfer, A., Schüssler, M., Solanki, S. K., Vögler, A., Katsukawa, Y., & Tsuneta, S. 2008, A&A, 484, L17
Frenkiel, F. N., & Schwarzschild, M. 1955, ApJ, 121, 216
Frutiger, C., Solanki, S. K., Fligge, M., & Bruls, J. H. M. J. 2000, A&A, 358, 1109
Gandorfer, A. 2005, The Second Solar Spectrum: A High Spectral Resolution Polarimetric Survey of Scattering Polarization at the Solar Limb in Graphical Representation,, Vol. III: 3160 Å to 3915 Å (Zürich: vdf Hochschulverlag)
Gandorfer, A., et al. 2010, Sol. Phys., in press (arXiv:1009.1037)
Hirzberger, J., Feller, A., Riethmüller, T. L., Gandorfer, A., & Solanki, S. K. 2010, A&A, submitted
Kurucz, R. 1993, ATLAS9 Stellar Atmosphere Programs and 2 km s^{-1} Grid, Kurucz CD-ROM No. 13 (Cambridge, MA: Smithsonian Astrophysical Observatory)
Löfdahl, M. G., & Scharmer, G. B. 1994, A&AS, 107, 243
Martínez Pillet, V., et al. 2010, Sol. Phys., in press (arXiv:1009.1095)
Mathew, S. K., Zakharov, V., & Solanki, S. K. 2009, A&A, 501, L19
Nordlund, Å., Stein, R. F., & Asplund, M. 2009, Living Rev. Sol. Phys., 6, 2
Sánchez Cuberes, M., Bonet, J. A., & Vázquez, M. 2000, ApJ, 538, 940
Sobotka, M., Vázquez, M., Sánches Cuberes, M., Bonet, J. A., & Hanslmeier, A. 2000, ApJ, 544, 1155
Solanki, S. K. 1987, PhD thesis, ETH Zürich
Solanki, S. K., & Unruh, Y. C. 1998, A&A, 329, 747
Solanki, S. K., et al. 2010, ApJ, 723, L127
Strom, S. E., & Kurucz, R. 1966, AJ, 71, 181
Vargas Domínguez, S. 2008, PhD thesis, Instituto de Astrofísica de Canarias, La Laguna
Vögler, A., Shelyag, S., Schüssler, M., Cattaneo, F., Emonet, T., & Linde, T. 2005, A&A, 429, 335
Wedemeyer-Böhm, S., & Rouppe van der Voort, L. 2009, A&A, 503, 225